INSTITUTE OF PHYSICS PUBLISHING and INTERNATIONAL ATOMIC ENERGY AGENCY NUCLEAR FUSION

Nucl. Fusion **45** (2005) 477–484 doi:10.1088/0029-5515/45/6/009

Transition from weak to strong energetic ion transport in burning plasmas

F. Zonca[1], S. Briguglio[1], L. Chen[2], G. Fogaccia[1] and G. Vlad[1]

[1] ENEA C. R. Frascati, C.P. 65, 00044 Frascati, Rome, Italy
[2] Department of Physics and Astronomy, University of California, Irvine, CA 92717-4575, USA

Received 9 December 2004, accepted for publication 3 May 2005
Published 24 May 2005
Online at stacks.iop.org/NF/45/477

Abstract
The change in nonlinear energetic particle mode (EPM) dynamics that accompanies the transition from weak to strong energetic ion transport is discussed in this work. It is demonstrated that the nonlinear threshold in fast ion energy density for the onset of strong convective transport occurring in avalanches is close to the linear EPM excitation threshold. This phenomenology is strictly related to the resonant character of the modes, which tend to be radially localized where the drive is strongest. After the convective loss phase, during which nonlinear EPM mode structure is displaced outwards, fast ion transport continues owing to diffusive processes. Theoretical analyses, presented here, are the basis for consistency analyses of operation scenarios in proposed burning plasma experiments. Comparisons between theoretical predictions and both simulation and experimental results are also briefly discussed.

PACS numbers: 52.35.Bj, 52.35.Mw, 52.55.Pi, 52.65.Ww

1. Introduction

A burning plasma is a self-organized system, where collective effects associated with fast ions (MeV energies) and charged fusion products (from now on referred to as fast or energetic ions) may alter their confinement properties and even jeopardize the achievement of ignition. Even if this extreme condition is to be strictly avoided for machines operating with burning plasmas, it is a crucial issue to consider the possible detrimental effect of collective mode excitations on the confinement properties of both fusion alphas and energetic ions for two main reasons: (i) these particles may be scattered by collective modes and eventually be lost before they transfer their energy to the thermal plasma via Coulomb collisions, thereby decreasing the fusion yield; (ii) energy and momentum fluxes owing to collective losses may lead to significant wall loading and damaging of plasma facing materials. These issues are of both academic and practical interest, since their investigation provides a detailed understanding of fundamental processes underlying collective behaviours of fusion products and of the accessible and relevant operation regimes of burning plasmas.

In the absence of a burning plasma experiment, precious information about the fundamental dynamic behaviour of fast ions in these conditions can be obtained by theoretical analyses, numerical simulations and by experimental studies of the fast ion tails produced by strong external heating sources, such as ion cyclotron resonant heating (ICRH) and neutral beam injection (NBI). Detailed comparisons between fundamental theories, numerical studies and experimental results are necessary to produce reliable extrapolations for next step fusion devices.

Simulation results indicate that above the threshold for the onset of resonant energetic particle modes (EPMs) [1], strong fast ion transport occurs in avalanches [2] (see figure 1). Such strong transport events occur on time scales of a few inverse linear growth rates (generally, 100–200 Alfvén times) and have a ballistic character [3] that basically differentiates them from the diffusive and local nature of weak transport. Meanwhile, numerical simulations have demonstrated that Alfvén Cascades in JET [4] are consistent with both weak and strong fast ion transport [5]. Recently, experimental observations on the JT-60U tokamak have also confirmed macroscopic and rapid (in the sense discussed above) energetic particle radial redistributions in connection with the so-called abrupt large amplitude events (ALE) [6–8]. Therefore, it is crucial to theoretically assess the potential impact of fusion product avalanches on burning plasma operation in the perspective of direct comparisons of those predictions with experimental evidence.

Here we analyse the nonlinear EPM dynamics in the case where the characteristic spatial scale length of fast ion energy density, L_p, is longer than the EPM perpendicular wavelength, i.e. $k_\perp L_p \gg 1$. This condition is necessary to observe the avalanche phenomenon as in figure 1, i.e. as the propagation of an unstable front [2]. Figure 1 refers to a JET-like

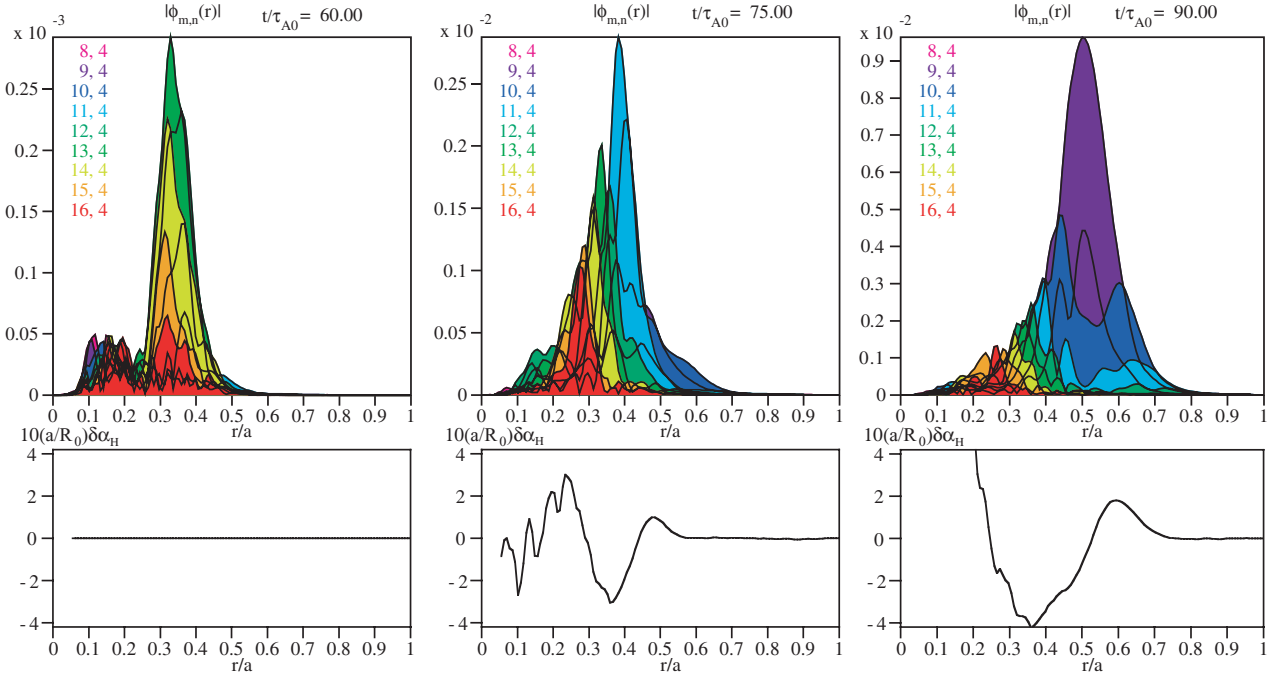

Figure 1. Time evolution of the EPM radial structure, decomposed in poloidal Fourier harmonics. Here, $\tau_{A0} = R_0/v_{A0}$, with R_0 the tokamak major radius and v_{A0} the on axis Alfvén speed. The toroidal mode number is $n = 4$. The rescaled nonlinear modification, $10(a/R_0)\delta\alpha_H$, of the energetic particle $\alpha_H = -R_0 q^2(\mathrm{d}\beta_H/\mathrm{d}r)$ is also shown [2], with a the tokamak minor radius.

reversed magnetic shear equilibrium with the minimum of the safety factor at $r/a = 0.53$ (see section 4). However, besides considering $k_\perp L_p \gg 1$, the analysis presented in sections 2 and 3 is generally applicable within the assumptions of tokamak equilibria with shifted circular magnetic surfaces and of wave–particle interactions dominated by the precession resonance, which is made for the sake of simplicity and could be easily dropped [9, 10]. The JET-like reversed magnetic shear equilibrium, assumed in figure 1, is then considered in section 4 as a simple yet relevant paradigm case to study.

The change in nonlinear EPM dynamics that accompanies the transition from weak to strong energetic ion transport is discussed in this work. It is demonstrated that the nonlinear threshold in fast ion energy density for the onset of avalanches is close to the linear EPM excitation threshold. This phenomenology is strictly related to the resonant character of the modes, which tend to be radially localized where the drive is strongest [9, 10]. When the nonlinear threshold is exceeded, the EPM envelope propagates radially for two reasons: the radial dispersiveness of the mode and the rapid redistribution of the energetic particle source. These two effects can be viewed as a manifestation of linear and nonlinear EPM radial group velocities, respectively. As it propagates, the EPM radial envelope is convectively amplified owing to resonant wave–particle interactions, which are responsible for the secular motion of the unstable front as well and, ultimately, of the avalanching process [2, 11–13]. After the convective loss phase, during which nonlinear EPM mode structure is displaced outwards, fast ion transport continues owing to diffusive processes [12, 13]. Theoretical analyses, presented here, are the basis for consistency analyses of operation scenarios in proposed burning plasma experiments [13–15]. Comparisons between theoretical predictions and both simulation [13–16] and experimental [17, 18] results are also briefly discussed.

2. Background

Our analysis refers to the nonlinear dynamic evolution of a single-n, i.e. a single toroidal mode number, coherent shear Alfvén wave, strongly driven in the presence of an isotropic fusion alpha particle population. For the sake of simplicity, we consider a low-β and large aspect ratio tokamak plasma with circular magnetic surfaces. Thus, the ratio of thermal to magnetic energy densities, $\beta = 8\pi P/B_0^2 \ll 1$, $B = B_0 R_0/R$ and the torus minor/major radii are such that $a/R_0 \ll 1$. Meanwhile, we can consider a simple (s, α) model equilibrium, with s the magnetic shear and $\alpha = -R_0 q^2(\mathrm{d}\beta/\mathrm{d}r)$, and assume a straight magnetic field line toroidal coordinate system (r, θ, ϕ), with $q(r) = (\boldsymbol{B}\cdot\boldsymbol{\nabla}\phi/\boldsymbol{B}\cdot\boldsymbol{\nabla}\boldsymbol{\theta})$ the safety factor.

As stated in the introduction, here, we analyse the nonlinear EPM dynamics in the case where the characteristic spatial scale length of fast ion energy density, L_p, is longer than the EPM poloidal wavelength, i.e. for $|k_\theta L_p| \gg 1$, or, equivalently, $nq \gg 1$. This is a necessary condition for observing the avalanche phenomenon of figure 1 as the propagation of an unstable front [2]. At longer EPM perpendicular wavelengths ($nq \gtrsim 1$), the fast ion transport may still have a ballistic character [3], but the radial mode structure is typically less variable than at $nq \gg 1$, owing to the poorer poloidal harmonic content of the mode, even when its amplitude is rapidly changing because of energetic particle radial redistributions. This appears to be the case of low toroidal mode number ALEs in the toroidal Alfvén eigenmode (TAE) [19] frequency range, for which the mode

frequency is nearly unchanged during bursts, but the amplitude rapidly varies in few wave cycles because of changes in the fast particle distribution function [20]. This observation confirms that the most evident signature of $nq \gtrsim 1$ bursting mode activity is given by rapid fast ion redistributions in phase space, similar to the *fishbone* case [21, 22], which is the historical paradigm for such strong energetic particle secular transport events [3]. These fast transports are usually difficult to measure directly unless they are accompanied by global losses or indirectly sampled by sudden drops in neutron fluxes. Characterizing such events via temporal behaviours of mode traces is difficult as well, since fast frequency sweeping phenomena cover nearly all time scales between those that are typical of core transport up to burst durations of the order of the real frequency spread. Thus, characterization of rapid bursting activities is a challenge for both theory and experiment and will require the study of nonlinear mode and particle dynamics on the same footing. Despite the typical weaker variability in the $nq \gtrsim 1$ than in the $nq \gg 1$ EPM radial mode structure, the longer poloidal wavelength fluctuations shape can still reflect the energetic particle radial profile, depending on the considered scenario, as shown in [13–16] and in recent numerical simulations [23, 24] of $n = 1$ fast frequency sweeping modes in JT-60U [6–8]. However, the $nq \gg 1$ nonlinear EPM dynamics sufficiently above threshold (as discussed in the introduction) is characterized by the typical signature of radial propagation of an unstable front, as in figure 1. This behaviour, if detected by high space and time resolution internal fluctuation measurements [25], could provide further evidence of fast ion redistributions. The $nq \gg 1$ EPM case is analysed in the rest of this work.

The nonlinear dynamics of a single-n coherent shear Alfvén wave is affected via both local and global phenomena. In the first category, the idea of mode saturation via wave–particle trapping [26, 27] has been successfully applied to explain pitchfork splitting of TAE spectral lines [28]. However, other physical mechanisms can be important, depending on the parameter regimes, as Compton scattering off the thermal ions [29] and mode–mode couplings generating a nonlinear frequency shift which may enhance the interaction with the shear Alfvén continuous spectrum [30, 31]. All these phenomena are local, in the sense, they either locally distort the fast ion distribution function because of quasi-linear wave–particle interactions [26, 27], or locally enhance the mode damping either via nonlinear wave–particle [29] or wave–wave interactions [30, 31]. For such a reason, the radial mode structure providing the envelope of the poloidal Fourier harmonics that compose the wave field—see equation (5)—never enters in all these treatments.

Intuitively speaking, the relevance of local phenomena in the nonlinear dynamics of a single-n coherent shear Alfvén wave near marginal stability [32] is readily understood. However, for a resonant mode like the EPM, which is localized where the drive is strongest [9, 10], global readjustments in the energetic particle drive are expected to be important as well. In the following, we will determine under what conditions global phenomena are relevant for EPM nonlinear dynamics and show that these become important right above the linear excitation threshold for the mode. Accounting for local and global phenomena on the same footing is extremely complex and, in this respect, numerical simulations appear to be the optimal tool for such analyses [12–16]. Hereafter, we neglect local phenomena and consider only global nonlinear EPM dynamics. Our findings will be checked for consistency *a posteriori*.

In the presence of global equilibrium profile changes, the nonlinear dynamics of a single-n coherent EPM can be affected by both $\boldsymbol{E}\times\boldsymbol{B}$ shearing owing to spontaneously generated zonal flows and by nonlinear distortions of the energetic ion source. Of these two processes, the latter is dominant for $(\alpha_{\rm H}/\beta_{\rm i})(T_{\rm i}/T_{\rm H}) \gg \epsilon^{3/2}$ [33], where $\alpha_{\rm H} = -R_0 q^2 ({\rm d}\beta_{\rm H}/{\rm d}r)$, $T_{\rm H}$ is the fast ion thermal energy, $\epsilon = r/R_0$, r is the radial position where the EPM is localized and $\beta_{\rm i}$ and $T_{\rm i}$ are the thermal ion β and temperature. This condition is typically satisfied for a resonantly excited EPM. Thus, in the following, we concentrate on the fast ion source nonlinear distortions. More specifically, we analyse these phenomena in the early nonlinear phase, when avalanching occurs [2, 16]. In the late nonlinear phase, besides the fast ion diffusion in the saturated field, radial fragmentation of the coherent EPM eddies can be spontaneously driven by modulational instability of the mode radial envelope due to radial modulations in the energetic particle source. This aspect is analysed in [33]. We now proceed with explicit calculations of the nonlinear fast ion global equilibrium profile changes.

3. Theoretical analyses

The theoretical framework of our analysis is that of [11, 33]; i.e. we decompose the fluctuating particle distribution function into adiabatic and nonadiabatic responses as [34]

$$\delta F_k = \frac{e}{m}\delta\phi_k \frac{\partial}{\partial v^2/2} F_0 + \sum_{\boldsymbol{k}_\perp} \exp\left(-{\rm i}\boldsymbol{k}_\perp \cdot \frac{\boldsymbol{v}\times\boldsymbol{b}}{\omega_{\rm c}}\right)\overline{\delta H}_k, \quad (1)$$

where notation is standard and the subscripts H for the energetic ions have been dropped unless needed to avoid confusion. The nonadiabatic response of the particle distribution function, $\overline{\delta H}_k$, is obtained from the nonlinear gyrokinetic equation [34]:

$$\begin{aligned}(\partial_t + v_\parallel\partial_\ell + {\rm i}\omega_{\rm d})_k \overline{\delta H}_k &= {\rm i}\frac{e}{m} Q F_0 J_0(\gamma)\left(\delta\phi_k - \frac{v_\parallel}{c}\delta A_{\parallel k}\right)\\ &\quad -\frac{c}{B}\boldsymbol{b}\cdot(\boldsymbol{k}''_\perp\times\boldsymbol{k}'_\perp)J_0(\gamma')\left(\delta\phi_{k'} - \frac{v_\parallel}{c}\delta A_{\parallel k'}\right)\overline{\delta H}_{k''},\\ Q F_0 &= \omega_k \frac{\partial F_0}{\partial v^2/2} + \boldsymbol{k}\cdot\frac{\boldsymbol{b}\times\boldsymbol{\nabla}}{\omega_{\rm c}} F_0, \end{aligned} \quad (2)$$

where $\delta\phi_k$ and $\delta A_{\parallel k}$ are the scalar and parallel vector potentials, $\partial_\ell = \boldsymbol{b}\cdot\boldsymbol{\nabla}$, $\omega_{\rm d}$ is the magnetic drift frequency, $\gamma = k_\perp v_\perp/\omega_{\rm c}$ and $\boldsymbol{k}_\perp = \boldsymbol{k}'_\perp + \boldsymbol{k}''_\perp$.

The present approach is based on treating hot particle distribution consisting of a background one plus a perturbation on meso time and space scales: thus the background distribution is frozen in time. To solve equation (2) for the nonlinear modification of the equilibrium fast particle distribution function in the presence of a coherent EPM, we adopt the procedure of [35]. Thus, indicating with $\overline{\delta H}_{\rm z}$ the $(m = 0, n = 0)$ (*zonal*) energetic ion response, we have

$$\begin{aligned}\overline{\delta H}_{\rm z} &= \exp(-{\rm i}Q_{\rm z})H_{\rm z},\\ Q_{\rm z} &= \frac{q}{(r/R_0)}k_{\rm z}\frac{v_\parallel}{\omega_{\rm c}},\end{aligned} \quad (3)$$

where $\boldsymbol{B}\cdot\boldsymbol{\nabla}H_z = 0$ and $k_z = (-\mathrm{i}\partial_r)$ is the radial wave vector of nonlinear equilibrium profile changes, as denoted by the subscript z, which stands for *zonal*. Equation (2) is then reduced to a 'quasilinear' evolution equation for the meso-scale H_z,

$$\frac{\partial}{\partial t}H_z = \sum_{\boldsymbol{k}_z=\boldsymbol{k}'+\boldsymbol{k}''}\mathrm{i}\frac{c}{B_0}k'_\theta \times\frac{\partial}{\partial r}\overline{\left[\mathrm{e}^{\mathrm{i}Q_z}J_0(\gamma')\left(\delta\phi_{k'}-\frac{v_\parallel}{c}\delta A_{\parallel k'}\right)\overline{\delta H}_{k''}\right]}, \tag{4}$$

with $k'_\phi = -k''_\phi$, $k'_\theta = -k''_\theta$ and $\overline{(\cdots)} = \int(\mathrm{d}\ell/v_\parallel)(\cdots)/\int(\mathrm{d}\ell/v_\parallel)$, ℓ being the arc length along $\boldsymbol{B}$ [35]. In order to make further analytic progress and discuss the EPM nonlinear dynamic evolution, we consider a simple case in which the dominant wave–particle interactions are described via the precession resonance (see [14, 15]) and assume that trapped particles move with a harmonic motion about the torus midplane, i.e. they behave as deeply trapped particles. We now introduce the following *ballooning* representation of the EPM mode structure:

$$\frac{e_\mathrm{H}}{T_\mathrm{H}}\delta\phi_k = \mathrm{e}^{\mathrm{i}n\phi}\sum_m \mathrm{e}^{-\mathrm{i}m\theta}\left(\int_{-\infty}^{\infty}\mathrm{e}^{-\mathrm{i}(nq-m)\eta}\Phi_0(\eta,\theta_k)\mathrm{d}\eta\right) \times\frac{A(r,t)}{\sqrt{2\pi}}, \tag{5}$$

where η is the extended poloidal angle, $\theta_k = (-\mathrm{i}/nq')\partial_r$ acting on the EPM envelope $A(r,t)$ [36] and $\Phi_0(\eta,\theta_k)$ is the ballooning EPM eigenfunction with the same normalizations chosen in [9]; i.e. its large $|\eta|$ behaviour can be written as

$$\Phi_0(\eta,\theta_k) = \frac{[a^{(\pm)}\cos(\eta/2)+b^{(\pm)}\sin(\eta/2)]}{\{1+[s(\eta-\theta_k)-\alpha\sin\eta]^2\}^{1/2}} \times\mathrm{e}^{(-\epsilon_0(\omega^2/\omega_\mathrm{A}^2)a^{(\pm)}b^{(\pm)}\eta)}. \tag{6}$$

Here, $a^{(\pm)} = \{1-\epsilon_0^{-1}[1-\omega_\mathrm{A}^2/(4\omega^2)]\}^{1/2}$, $b^{(\pm)} = \pm\{1+\epsilon_0^{-1}[1-\omega_\mathrm{A}^2/(4\omega^2)]\}^{1/2}$, $(\pm)$ stands for (positive/negative) η, $\epsilon_0 = 2(\epsilon+\Delta')$, Δ' is the radial derivative of the Shafranov shift and $\omega_\mathrm{A} = v_\mathrm{A}/(qR_0)$ is the local value of the Alfvén frequency. Then, the linear energetic particle response in the ballooning representation is

$$\overline{\delta H}_k \simeq -\left(\frac{e}{m}\right)J_0(\gamma)\frac{QF_0}{\omega} \times\left[\Phi_0(\eta,\theta_k)-J_0(Q_{k0})\frac{\bar\omega_\mathrm{d}\mathrm{e}^{-\mathrm{i}Q_k}}{\bar\omega_\mathrm{d}-\omega}\Phi_{0\mathrm{c}}(\eta,\theta_k)\right], \tag{7}$$

where Q_k stands for Q_z with k_z substituted by k_r and with θ dependences mapped into η, Q_{k0} is Q_k computed at $\theta = 0$ and $\Phi_{0\mathrm{c}}(\eta,\theta_k)$ is $\Phi_0(\eta,\theta_k)$ with only $\propto\cos(\eta/2)$ dependences included. Note that, here, we have assumed that finite banana-width effects are dominated by geodesic curvature for finite magnetic shear [9, 37–39]. Substituting back this expression into equation (4), we are still left with residual fast radial dependences on the k_r^{-1} scale. In the present case, we are interested in nonlinear energetic particle distortions to the equilibrium fast ion pressure gradient on the k_z^{-1} scale, ordered as the EPM radial envelope width. We can, thus, further average equation (4) on the fast radial scale and we finally obtain

$$\frac{\partial}{\partial t}h_z = 2k_\theta^2\rho_\mathrm{H}^2\frac{\omega_{c\mathrm{H}}}{k_\theta}\frac{T_\mathrm{H}}{m_\mathrm{H}}\frac{\partial}{\partial r}\left[\mathrm{Im}\left(\frac{QF_0}{\omega}\frac{\bar\omega_\mathrm{d}}{\bar\omega_\mathrm{d}-\omega}\right)\Gamma^2|A|^2\right]_\mathrm{H}. \tag{8}$$

Here, h_z is the spatially averaged expression of H_z, ρ_H is the energetic ion Larmor radius and T_H is the fast ion thermal energy. Furthermore, with $\gamma = k_\theta(1+s^2\eta^2)^{1/2}(2\mu B_0)^{1/2}/\omega_\mathrm{c}$, μ the magnetic moment, $Q_{k0} = k_\theta\theta_\mathrm{b}s\eta q(v^2/2)^{1/2}\epsilon^{-1/2}/\omega_\mathrm{c}$ and θ_b the bounce angle,

$$\Gamma^2 = \int_{-\infty}^{\infty}J_0^2(\gamma)J_0^2(Q_{k0})\,|\Phi_{0\mathrm{c}}(\eta,\theta_k)|^2\,\mathrm{d}\eta \tag{9}$$

describes finite Larmor radius as well as the banana-width effects. Here, the finite orbit width effects owing to k_z are neglected since $|k_z| \ll |k_r|$.

The EPM dispersion relation can be always expressed in the form [9]

$$[D_\mathrm{R}(\omega,\theta_k;s,\alpha)+\mathrm{i}D_\mathrm{I}(\omega,\theta_k;s,\alpha)]\,A_0 = \delta W_{KT}A_0, \tag{10}$$

where we have extracted the rapid EPM oscillation frequency from the mode amplitude as $A(r,t) = A_0(r,t)\exp(-\mathrm{i}\omega_0 t)$, with $A_0(r,t)$ accounting for slow time variations only, i.e. $|\omega^{-1}\partial_t\ln A_0| \ll 1$. In equation (10), $\omega = \omega_0+\mathrm{i}\partial_t$ and $\theta_k = (-\mathrm{i}/nq')\partial_r$ are operators acting on $A_0(r,t)$, and both real, D_R, and imaginary part, D_I, of the dispersion function can be formally treated as the principal symbol of a pseudo-differential operator [9, 40, 41]. Furthermore, δW_{KT} is related to the fast ion contribution to the potential energy and can be written as [9]

$$\delta W_{KT} = \frac{2\pi^2\mathrm{e}^2}{mc^2}qR_0B_0\sum_{v_\parallel/|v_\parallel|=\pm}\int\mathrm{d}\left(\frac{v^2}{2}\right)\int\mathrm{d}\mu\frac{\bar\omega_\mathrm{d}^2}{k_\theta^2}\tau_\mathrm{B}\frac{QF_0}{\bar\omega_\mathrm{d}-\omega}, \tag{11}$$

where $\tau_\mathrm{B} = 2\pi/\omega_\mathrm{B} = 2\pi qR_0(2/v^2)^{1/2}\epsilon^{-1/2}$ is the bounce period of deeply trapped ions. Note that, equation (11) does not depend on the mode number, consistently with $s \approx 1$ and with the wavelength ordering $k_\theta\rho_\mathrm{H} \lesssim \epsilon \lesssim k_\theta\rho_\mathrm{BH} \lesssim \epsilon^{1/2} < 1$, assumed here, and corresponding to the most unstable conditions [9, 37–39] (ρ_BH is the fast ion banana width). Nonlinearly,

$$QF_0 \to QF_0+\frac{k_\theta}{\omega_\mathrm{c}}\frac{\partial}{\partial r}h_z \tag{12}$$

and the EPM dispersion relation, equation (10), is readily generalized. To explicitly compute equation (11), we choose an isotropic slowing down distribution function, which has a cut-off at the fusion energy E_fus and is normalized to the fast alpha particle pressure P_H considering $E_\mathrm{fus} \gg E_\mathrm{c}$, with E_c the critical energy [42]:

$$F_0 = \frac{3P_\mathrm{H}}{4\pi E_\mathrm{fus}}\frac{1}{v^3+(2E_\mathrm{c}/m_\mathrm{H})^{3/2}}. \tag{13}$$

In this way, defining $\bar\omega_{\mathrm{d}F}$ as $\bar\omega_\mathrm{d}$ computed at E_fus, we obtain

$$\delta W_{KT} = \frac{3\pi\epsilon^{1/2}}{4\sqrt{2}}\alpha_\mathrm{H}\left[1+\frac{\omega}{\bar\omega_{\mathrm{d}F}}\ln\left(\frac{\bar\omega_{\mathrm{d}F}}{\omega}-1\right)+\mathrm{i}\pi\frac{\omega}{\bar\omega_{\mathrm{d}F}} +\mathrm{i}\pi\frac{\omega}{\bar\omega_{\mathrm{d}F}}k_\theta^2\rho_\mathrm{H}^2\frac{T_\mathrm{H}}{m_\mathrm{H}}\frac{1}{\alpha_\mathrm{H}A_0}\partial_t^{-1}A_0\partial_r^2\partial_t^{-1}\left(\alpha_\mathrm{H}|A_0|^2\right)\right]. \tag{14}$$

Here, ∂_t^{-1} is the standard notation for the inverse of ∂_t and we have kept the nonlinear modification to the imaginary part of δW_{KT} only, consistently with the ordering $|\omega^{-1}\partial_t| \ll 1$. Furthermore, we have assumed that the nonlinear time scale is sufficiently long to avoid destroying resonant wave–particle interactions. Note that using the ∂_t^{-1} notation is consistent with the time scale separation $|\omega^{-1}\partial_t| \ll 1$ and reminds us of having used a formal treatment of pseudo-differential operators in equations (10) and (11) [9, 40, 41]. Substituting back into equation (10), we finally obtain

$$\begin{aligned}[D_{\mathrm{R}}(\omega,\theta_k;s,\alpha)+\mathrm{i}D_{\mathrm{I}}(\omega,\theta_k;s,\alpha)]\,\partial_t A_0 \\ = \frac{3\pi\epsilon^{1/2}}{4\sqrt{2}}\alpha_{\mathrm{H}}\left[1+\frac{\omega}{\bar\omega_{\mathrm{d}F}}\ln\left(\frac{\bar\omega_{\mathrm{d}F}}{\omega}-1\right)+\mathrm{i}\pi\frac{\omega}{\bar\omega_{\mathrm{d}F}}\right]\partial_t A_0 \\ +\mathrm{i}\pi\frac{\omega}{\bar\omega_{\mathrm{d}F}}A_0\frac{3\pi\epsilon^{1/2}}{4\sqrt{2}}k_\theta^2\rho_{\mathrm{H}}^2\frac{T_{\mathrm{H}}}{m_{\mathrm{H}}}\partial_r^2\partial_t^{-1}\left(\alpha_{\mathrm{H}}|A_0|^2\right). \qquad (15)\end{aligned}$$

Equation (15) can be taken as the starting point for detailed analyses of avalanche dynamics induced by EPM, which will be reported elsewhere. In the next section, we present a discussion of equation (15) in the *local limit* and compare our findings with results from numerical simulations.

Note that equation (15) is readily generalized to include both precession-bounce as well as transit wave–particle resonances by extending equation (10) to these cases [9] and by using the approach of [33] to calculate the corresponding nonlinear energetic particle zonal response, h_{z}.

4. Local limit

Consider again the case of figure 1, referring to a JET-like q-profile in reversed shear experiments with Alfvén Cascade excitation [4] and a model Maxwellian fast ion distribution function [2, 16]. Figure 2 shows the EPM intensity contour plots (left frames) and the corresponding fast ion surface density (right frames) for the linearly unstable and saturated phases of the EPM avalanche. The shear Alfvén continuum is emphasized in black in the background of contour plots, with the visible effect of the minimum-q surface at $r/a \simeq 0.53$. Despite the difference in the fast ion sources—isotropic Maxwellian versus the isotropic slowing down assumed here—we use figures 1 and 2 as a typical paradigm for EPM avalanches owing to trapped energetic ions; i.e. the case for which, under simplifying assumptions, equation (15) was derived. Specifically, it can be shown that the $n = 4$ mode in figure 1 is driven mainly by the precession resonance ($\omega \simeq \bar\omega_{\mathrm{d}} \propto nq$) at the radial position, where, the drive is strongest [13–15].

In order to investigate the nonlinear dynamics of EPM avalanches, it is instructive to solve equation (15) in the local limit. In fact, the narrow structure of the EPM envelope suggests that we assume $|\theta_k| \ll 1$. Meanwhile, we can also consider that—near the peak of fast particle drive at r_0—radial dependences of the dispersion function are mainly due to the fast ion source profile, $\alpha_{\mathrm{H}} = \alpha_{\mathrm{H0}}\exp(-x^2/L_{\mathrm{p}}^2)$, with $x = (r - r_0)$ and L_{p} the characteristic α_{H} scale length. Finally, q-profile changes account for the dominant radial variation of the shear Alfvén continuum and $\bar\omega_{\mathrm{d}F}$.

In the linear limit, the mode frequency is determined by balancing D_{R} with $\mathrm{Re}\,\delta W_{KT}$:

$$D_{\mathrm{R}}(\omega_0,\theta_k=0,s,\alpha) = \mathrm{Re}\,\delta W_{KT}|_{x=0,\omega_0}. \qquad (16)$$

Meanwhile, the mode growth rate, γ_L, is given by the competition between energetic particle drive $\propto \mathrm{Im}\,\delta W_{KT}|_{x=0,\omega_0}$ and continuum damping $\propto D_{\mathrm{I}}(\omega_0,\theta_k=0,s,\alpha)$:

$$\gamma_L = \left(\mathrm{Im}\,\delta W_{KT} - D_{\mathrm{I}}\right)\left[\partial_{\omega_0}\left(D_{\mathrm{R}} - \mathrm{Re}\,\delta W_{KT}\right)\right]^{-1}\Big|_{x=0,\theta_k=0,\omega_0}. \qquad (17)$$

The radial dispersiveness, $\propto\theta_k^2$, balancing the energetic ion profile effects, $\propto(\exp(-x^2/L_{\mathrm{p}}^2)-1) \simeq -x^2/L_{\mathrm{p}}^2$, finally gives a typical radial envelope width $\Delta \approx (L_{\mathrm{p}}/k_\theta)^{1/2}$ and a complex frequency shift of $O(k_\theta^{-1}L_{\mathrm{p}}^{-1})$ [10].

Nonlinearly, equation (15) shows that the EPM reduces the drive (α_{H}) where the envelope is maximal and, at the same time, strengthens it in the nearby region, where $\partial_r^2 \ln|A|^2 > 0$. This behaviour is clearly visible in the lower frames of figure 1. In order to maximize the drive, one readily sees that the EPM changes its radial localization according to

$$\left(\frac{x_0}{L_{\mathrm{p}}}\right) = \gamma_L^{-1}k_\theta\rho_{\mathrm{H}}\left(\frac{T_{\mathrm{H}}}{M_{\mathrm{H}}}\right)^{1/2}\left(\frac{|A_0|}{W_0}\right), \qquad (18)$$

x_0 being the radial position of the maximum EPM amplitude, W_0 indicating the typical EPM radial width in the nonlinear regime and having used γ_L^{-1} to estimate the characteristic time in the early nonlinear phase. This displacement is an avalanche in the sense that the mode moves radially, following an unstable propagating front [11], and it is directed outwards since continuum damping is a decreasing function of (r/a) up to the minimum-q surface and then increasing again, as is evident from figure 2. This fact clearly facilitates the secular motion up to the minimum-q surface, since the decreasing continuum damping partially compensates the weakening of the drive as a result of the local phenomena discussed at the beginning of section 2. Furthermore, this analysis provides an explanation of the reason why the EPM exhibits the natural tendency to merge into a Cascade mode at the minimum-q surface at the end of the convective amplification [5]. Note that the secular motion scales linearly with the mode amplitude, consistently with the numerical simulation in figure 1, as it is shown in figure 3. There, the first and lowest amplitude point still corresponds to an initial local growth of the EPM. The linear scaling is expected for the following three points, for which profile variations effects on q, L_{p} and W_0 can be neglected (see equation (18)). Meanwhile, the real mode frequency still satisfies equation (16) computed at x_0. Therefore, the nonlinear frequency shift during the avalanche phase is

$$\Delta\omega = s\,\bar\omega_{\mathrm{d}F}|_{x_0}\left(\frac{x_0}{r}\right)\left(\frac{\omega_0}{\bar\omega_{\mathrm{d}F}|_{x=0}}\right), \qquad (19)$$

which, combined with equation (18), gives $\Delta\omega \propto |A_0|$ as well. It is worth recalling that the frequency *chirping*, described by equation (19), is strictly connected with the resonant character of the mode as well as with equilibrium profile changes. For weak magnetic shear, e.g. the real mode frequency shift can be negligible. The frequency chirping obviously depends on the type of wave–particle resonance which is most relevant

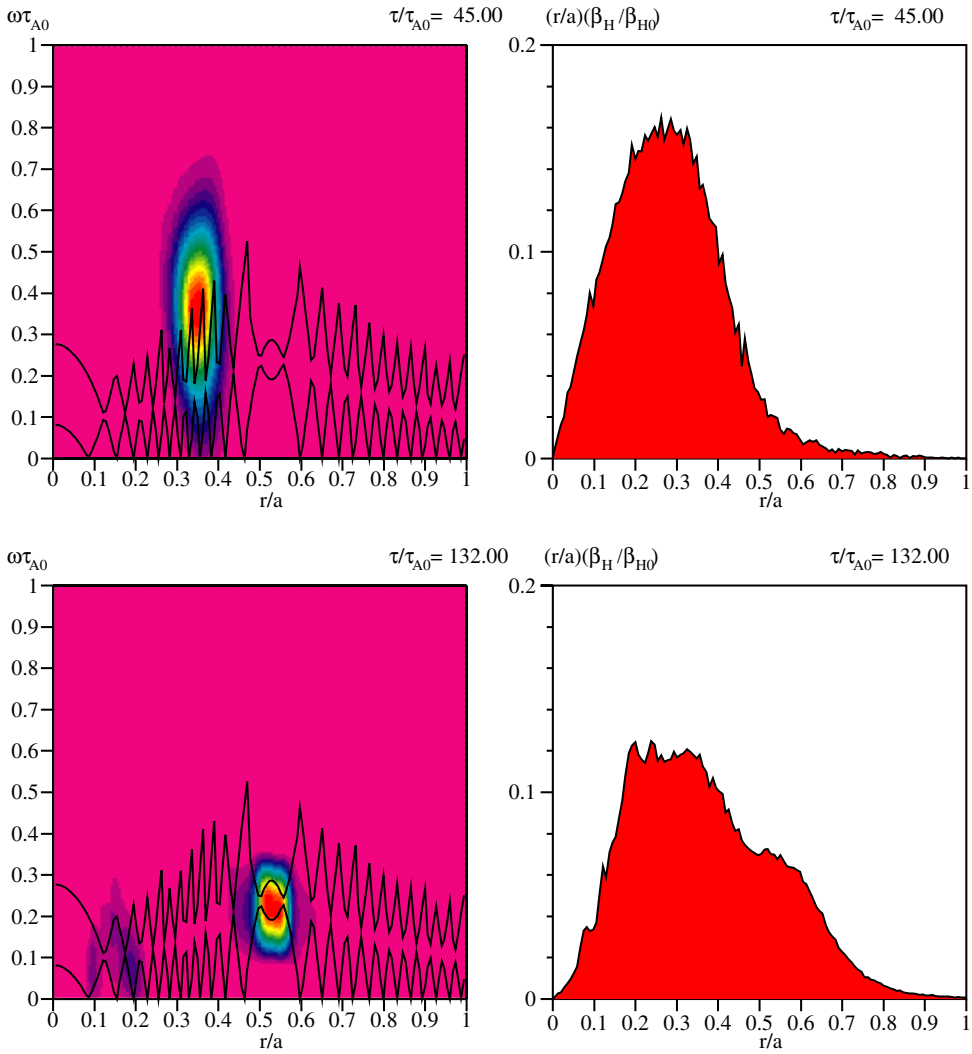

Figure 2. Linearly unstable (top) and saturated (bottom) phases for on axis $\beta_{\mathrm{H0}} = 0.025$ and the other profiles as discussed in [2, 16].

for the mode excitation. *Exempli gratia*, for the transit resonance (see discussion at the end of section 3), as in the case of ALE on JT-60U [6–8, 20], $\omega_t \propto T_{\mathrm{H}}^{1/2}/q$ and the behaviour is expected to be quite different than for the precession resonance, $\bar{\omega}_{\mathrm{d}} \propto nqT_{\mathrm{H}}$.

A posteriori, we may estimate the strength of EPM drive required to trigger an avalanche by the value of the convective displacement, $\bar{x}_0$, given by equation (18), at the time the mode amplitude reaches the critical saturation value via wave–particle trapping, i.e. $\omega_{\mathrm{b}} \approx \gamma_L$ [26, 27, 32], with the wave–particle trapping frequency ω_{b} such that $\omega_{\mathrm{b}}^2 \approx k_\theta^2 \rho_{\mathrm{H}}^2 k_\theta (T_{\mathrm{H}}/m_{\mathrm{H}}) R_0^{-1} |A|$ [26]. We readily obtain $\bar{x}_0 \approx R_0 \gamma_L / (k_\theta \rho_{\mathrm{H}})(T_{\mathrm{H}}/m_{\mathrm{H}})^{-1/2} (\Delta^2/W_0)$. We can reasonably assume that the avalanching process is triggered when the EPM secular motion shifts its localization by one mode rational surface by the time the wave–particle trapping becomes important. Meanwhile, the avalanching process is expected to become increasingly strong when the EPM secular displacement reaches a typical global mode width. Thus, in the very early nonlinear phase, we may expect that a weak avalanche is triggered when $k_\theta \bar{x}_0 \gtrsim 1$, i.e.

$$1 \gg \frac{\gamma_L}{k_\theta \rho_{\mathrm{H}} (T_{\mathrm{H}}/m_{\mathrm{H}})^{1/2} R_0^{-1}} \gtrsim (k_\theta L_{\mathrm{p}})^{-1/2}, \qquad (20)$$

whereas strong avalanching is expected to occur for $\bar{x}_0 \gtrsim W_0$, i.e.

$$1 \gg \frac{\gamma_L}{k_\theta \rho_{\mathrm{H}} (T_{\mathrm{H}}/m_{\mathrm{H}})^{1/2} R_0^{-1}} \gtrsim \frac{W_0^2}{\Delta^2}. \qquad (21)$$

Note that $W_0^2/\Delta^2 \ll 1$ in equation (21) owing to the short scale of the nonlinear distortion, $\delta\alpha_{\mathrm{H}}$, in the equilibrium α_{H} profile, as it emerges from figure 1. Both equations (20) and (21) show that the onset for EPM-induced avalanches is close to the linear excitation threshold. If neither of these conditions is satisfied, EPM will saturate either via wave–particle trapping or other local phenomena, discussed at the beginning of section 2.

5. Discussions and conclusions

In this work, we have discussed the change in nonlinear EPM dynamics that accompanies the transition from weak

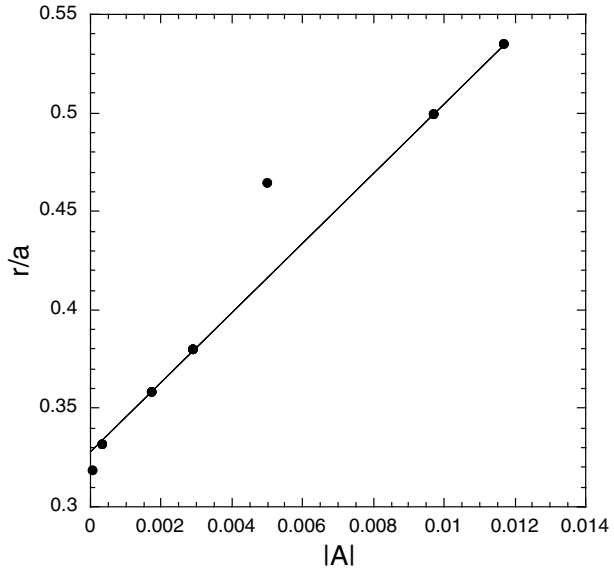

Figure 3. Radial position of the maximum EPM amplitude versus the peak amplitude itself, during the convective amplification process.

(diffusive) to strong (ballistic) energetic ion transport. The nonlinear threshold in fast ion energy density for the onset of strong convective transport, occurring in avalanches, is close to the linear EPM excitation threshold [16, 43].

The relevance of strong energetic particle transport due to EPM convective amplification in burning plasmas is discussed in [13–16]. However, it is worthwhile recalling that fusion product transport will depend on the dynamic formation processes of the reference equilibria, which can be influenced by weak Alfvén mode excitation near marginal stability [27, 28]. Certainly, experimental observations of rapid and macroscopic fast particle transports [44–50], like those associated with ALE on JT-60U [6–8, 20], suggest that it is possible to excite large amplitude Alfvénic modes with signatures similar to EPMs in situations of practical interest. These transport events are generally associated with fast frequency chirping that are evidently a result of nonlinear dynamic changes in the fast particle distribution [10, 20, 51], since they occur on characteristic times, which are shorter than the thermal transport time scale.

Slower chirping modes on the typical diffusion time of plasma current are widely observed [4, 52–55]. Under different names, mostly Alfvén Cascades [4, 54] and reversed shear-induced Alfvén eigenmodes (RSAEs) [55, 56], these modes are interpreted as shear Alfvén waves located near the accumulation points of the shear Alfvén continuum at the minimum-q surface owing to the degeneracy removal by either the presence of a finite fast ion population [57] or by higher order (in the inverse aspect ratio) toroidal equilibrium effects [56, 58]. These fluctuations are often accompanied by fast frequency sweeping modes. For example, it has been recently shown that there exists Alfvénic fluctuations, characterized by rapidly chirping frequency, which are observed in JET in connection with excitation of large amplitude Alfvén Cascades [17, 18]. On a standard spectrogram, these fluctuations appear as nearly vertical segments superimposed on the slower frequency change of the Alfvén Cascade or RSAE, giving a clear flavour of the different time scales involved [17, 18, 45, 52, 53, 55]. In the case of JET, the modes rapidly chirp downward in frequency and eventually merge into the spectral lines of Cascade modes (see figure 8 of [17]), similarly to the qualitative behaviour discussed above for EPM (see section 4). It must be pointed out, though, that in the JET case precession-bounce resonances are more likely to play a dominant role. From our analysis, it is evident that an essential role in the avalanche dynamics is played by wave–particle resonant interactions as well as by the shear Alfvén continuous spectrum. Therefore, dedicated modelling is required for quantitative comparisons between theory, simulation and experiments.

Acknowledgments

This work was partly supported by DoE Grants DE-94ER54271 and 54736, and NSF Grant ATM-033527.

References

[1] Chen L. 1994 *Phys. Plasmas* **1** 1519
[2] Zonca F., Briguglio S., Chen L., Fogaccia G. and Vlad G. 2002 *Proc. 19th Int. Conf. on Fusion Energy 2002 (Lyon, 2002)* (Vienna: IAEA) CD-ROM file TH/4-4 and http://www.iaea.org/programmes/ripc/physics/fec2002/html/fec2002.htm
[3] White R.B., Goldston R.J., McGuire K., Boozer A.H., Monticello D.A. and Park W. 1983 *Phys. Fluids* **26** 2958
[4] Sharapov S.E. *et al* 2001 *Phys. Lett.* A **289** 127
[5] Zonca F., Briguglio S., Chen L., Dettrick S., Fogaccia G., Testa D. and Vlad G. 2002 *Phys. Plasmas* **9** 4939
[6] Shinohara K. *et al* 2001 *Nucl. Fusion* **41** 603
[7] Shinohara K. *et al* 2002 *Nucl. Fusion* **42** 942
[8] Shinohara K. *et al* 2004 *Plasma Phys. Control. Fusion* **46** S31
[9] Zonca F. and Chen L. 1996 *Phys. Plasmas* **3** 323
[10] Zonca F. and Chen L. 2000 *Phys. Plasmas* **7** 4600
[11] Zonca F., Briguglio S., Fogaccia G. and Vlad G. 2003 Transition from weak to strong fusion product transport in burning plasmas *8th IAEA Technical Meeting on Energetic Particles in Magnetic Conf. Systems (San Diego, CA, 6–8 October 2003)*
[12] Vlad G., Briguglio S., Fogaccia G. and Zonca F. 2003 Alpha particle transport induced by Alfvénic instabilities in proposed burning plasma scenarios *8th IAEA Technical Meeting on Energetic Particles in Magnetic Conf. Systems (San Diego, CA, October 6–8 2003)*
[13] Vlad G., Briguglio S., Fogaccia G. and Zonca F. 2004 *Plasma Phys. Control. Fusion* **46** S81
[14] Vlad G., Briguglio S., Fogaccia G., Zonca F. and Schneider M. 2004 *Proc. 20th IAEA Fusion Energy Conf.* (Vienna: IAEA) Paper IT/P3-31, online publication available from Spring 2005
[15] Vlad G., Briguglio S., Fogaccia G., Zonca F. and Schneider M. 2004 Alfvénic instabilities driven by fusion generated alpha particles in ITER scenarios *Nucl. Fusion* **45** at press
[16] Briguglio S., Vlad G., Zonca F. and Fogaccia G. 2002 *Phys. Lett.* A **302** 308
[17] Pinches S.D. *et al* 2004 *Plasma Phys. Control. Fusion* **46** B187
[18] Sharapov S.E. *et al* 2004 *Proc. 20th IAEA Fusion Energy Conf.* (Vienna: IAEA) Paper EX/5-2Ra, online publication available from Spring 2005
[19] Cheng C.Z., Chen L. and Chance M.S. 1985 *Ann. Phys.* **161** 21
[20] Cheng C.Z. *et al* 2002 *Proc. 19th Int. Conf. on Fusion Energy 2002 (Lyon, 2002)* (Vienna: IAEA) CD-ROM file TH/7-1Rb and http://www.iaea.org/programmes/ripc/physics/fec2002/html/fec2002.htm

[21] Chen L., White R.B. and Rosenbluth M.N. 1984 *Phys. Rev. Lett.* **52** 1122
[22] Coppi B. and Porcelli F. 1986 *Phys. Rev. Lett.* **57** 2272
[23] Todo Y., Shinohara K., Takechi M. and Ishikawa M. 2003 *J. Plasma Fusion Res.* **79** 1107
[24] Todo Y., Shinohara K., Takechi M. and Ishikawa M. 2005 *Phys. Plasmas* **12** 012503
[25] Sharapov S.E. *et al* 2004 *Phys. Rev. Lett.* **93** 165001
[26] Berk H.L. and Breizman B.N. 1990 *Phys. Fluids* B **2** 2246
[27] Berk H.L., Breizman B.N. and Pekker M.S. 1997 *Plasma Phys. Rep.* **23** 778
[28] Fasoli A., Breizman B.N., Borba D., Heeter R.F., Pekker M.S. and Sharapov S.E. 1998 *Phys. Rev. Lett.* **81** 5564
[29] Hahm T.S. and Chen L. 1995 *Phys. Rev. Lett.* **74** 266
[30] Zonca F., Romanelli F., Vlad G. and Kar C. 1995 *Phys. Rev. Lett.* **74** 698
[31] Chen L., Zonca F., Santoro R.A. and Hu G. 1998 *Plasma Phys. Control. Fusion* **40** 1823
[32] Berk H.L., Breizman B.N. and Pekker M.S. 1996 *Phys. Rev. Lett.* **76** 1256
[33] Zonca F., Briguglio S., Chen L., Fogaccia G. and Vlad G. 2000 *Theory of Fusion Plasmas* ed J.W. Connor *et al* (Bologna: SIF) p 17
[34] Frieman E.A. and Chen L. 1982 *Phys. Fluids* **25** 502
[35] Rosenbluth M.N. and Hinton F.L. 1998 *Phys. Rev. Lett.* **80** 724
[36] Dewar R.J., Manickam J.L., Grimm R.C. and Chance M.S. 1981 *Nucl. Fusion* **21** 493
[37] Fu G.Y. and Cheng C.Z. 1992 *Phys. Fluids* B **4** 3722
[38] Berk H.L., Breizman B.N. and Ye H. 1992 *Phys. Lett.* A **162** 475
[39] Tsai S.T. and Chen L. 1993 *Phys. Fluids* B **5** 3284
[40] Zonca F., White R.B. and Chen L. 2004 *Phys. Plasmas* **11** 2488
[41] Zonca F., Chen L. and White R.B. 2004 *Theory of Fusion Plasmas* ed J.W. Connor *et al* (Bologna: SIF) p 3
[42] Stix T.H. 1972 *Plasma Phys.* **14** 367
[43] Briguglio S., Zonca F. and Vlad G. 1998 *Phys. Plasmas* **5** 3287
[44] Heidbrink W.W., Carolipio E.M., James R.A. and Strait E.J. 1995 *Nucl. Fusion* **35** 1481
[45] Kusama Y. *et al* 1999 *Nucl. Fusion* **39** 1837
[46] Bernabei S. *et al* 1999 *Phys. Plasmas* **6** 1880
[47] Fredrickson E.D. *et al* 2003 *Phys. Plasmas* **10** 2852
[48] Gryaznevich M.P. and Sharapov S.E. 2004 *Plasma Phys. Control. Fusion* **46** S15
[49] Fredrickson E.D. *et al* 2004 *Proc. 20th IAEA Fusion Energy Conf.* (Vienna: IAEA) Paper EX/5-3, online publication available from Spring 2005
[50] Heidbrink W.W. 2004 private communication
[51] Berk H.L., Breizman B.N. and Petviashvili N.V. 1997 *Phys. Lett.* A **234** 213
[52] Kusama Y. *et al* 1998 *Nucl. Fusion* **38** 1215
[53] Kimura H. *et al* 1998 *Nucl. Fusion* **38** 1303
[54] Snipes J.A. *et al* 2000 *Plasma Phys. Control. Fusion* **42** 381
[55] Takechi M. *et al* 2002 *Proc. 19th Int. Conf. on Fusion Energy 2002 (Lyon, 2002)* (Vienna: IAEA) CD-ROM file EX/W-6 and http://www.iaea.org/programmes/ripc/physics/fec2002/html/fec2002.htm
[56] Fukuyama A. and Akutsu T. 2002 *Proc. 19th Int. Conf. on Fusion Energy 2002 (Lyon, 2002)* (Vienna: IAEA) CD-ROM file TH/P3-14 and http://www.iaea.org/programmes/ripc/physics/fec2002/html/fec2002.htm
[57] Berk H.L., Borba D.N., Breizman B.N., Pinches S.D. and Sharapov S.E. 2001 *Phys. Rev. Lett.* **87** 185002
[58] Breizman B.N., Berk H.L., Pekker M.S., Pinches S.D. and Sharapov S.E. 2003 *Phys. Plasmas* **10** 3649